Phase field modeling of electrochemistry. II. Kinetics

J. E. Guyer,* W. J. Boettinger,† and J. A. Warren‡
Metallurgy Division, Materials Science and Engineering Laboratory, National Institute of Standards and Technology, Gaithersburg, Maryland 20899, USA

G. B. McFadden§
Mathematical and Computational Sciences Division, Information Technology Laboratory, National Institute of Standards and Technology, Gaithersburg, Maryland 20899, USA
(Received 11 August 2003; published 27 February 2004)

The kinetic behavior of a phase field model of electrochemistry is explored for advancing (electrodeposition) and receding (electrodissolution) conditions in one dimension. We previously described the equilibrium behavior of this model [J. E. Guyer, W. J. Boettinger, J. A. Warren, and G. B. McFadden, Phys. Rev. E **69**, 021603 (2004)]. We examine the relationship between the parameters of the phase field method and the more typical parameters of electrochemistry. We demonstrate ohmic conduction in the electrode and ionic conduction in the electrolyte. We find that, despite making simple, linear dynamic postulates, we obtain the nonlinear relationship between current and overpotential predicted by the classical ''Butler-Volmer'' equation and observed in electrochemical experiments. The charge distribution in the interfacial double layer changes with the passage of current and, at sufficiently high currents, we find that the diffusion limited deposition of a more noble cation leads to alloy deposition with less noble species.

DOI: 10.1103/PhysRevE.69.021604 PACS number(s): 81.15.Aa, 81.15.Pq, 82.20.Wt, 82.45.Qr

I. INTRODUCTION

In Ref. [1], we developed an equilibrium phase field model of an electrochemical system. In this paper, we examine the dynamic aspects of that model. Models of phase transformations can be broadly categorized into sharp or diffuse interface approaches. Sharp interface models treat the transition between phases as mathematically abrupt. Diffuse interface models assume that the phase interface has some finite thickness over which material properties vary smoothly. Both cases are simplifications of the physical interface between phases, in which properties vary over some finite, atomic-scale distance which is often smaller than assumed in diffuse interface models. Traditional equilibrium models of electrochemical interfaces take the interface between phases (the transition between ''electrode'' and ''electrolyte'') to be abrupt, but frequently consider the distribution of charge and electrostatic potential to be diffuse in the electrolyte, as by the Gouy-Chapman-Stern model [2]. Dynamic models of electrochemistry typically take the phase inteface to be abrupt and ignore the details of the charge distribution at the interface.

The phase field technique is one particular diffuse interface approach. The method employs a phase field variable, which is a function of position and time, to describe whether the material is one phase or another, e.g., solid or liquid. The behavior of this variable is governed by a partial differential equation that is coupled to the relevant transport equations for the material. The interface between the phases is described by smooth but highly localized changes of this variable. This approach avoids the mathematically difficult problem of applying boundary conditions at an interface whose location is part of the unknown solution. The phase field method is powerful because it can easily treat complex interface shapes and topology changes. Our long term goal is to treat the complex geometry, including void formation, that occurs during electrodeposition in vias and trenches for on-chip metallization and in the dendritic structures that form during battery recharging. Phase field methods will allow the rigorous examination of the interplay between current, potential gradients, curvature, and adsorption in intricate geometries.

There is a rich body of literature of sharp interface models of electrodeposition, which we will sketch briefly in Sec. II, but the application of diffuse interface techniques to the motion of electrochemical interfaces has been relatively limited. Dussault and Powell have applied phase field techniques to the modeling of electrochemical processes in steel slags [3,4], but their approach neglects the effects of charge at the interfacial double layer. As a result, they are able to model much larger domains and much longer time spans than we present here, but the essential physics of the electrocapillary interface is not examined. Wheeler, Josell, and Moffat have performed a level set analysis of so-called ''superconformal'' electrodeposition in high aspect ratio features, with particular emphasis on the role of additives [5]. Like phase field models, level set techniques allow the treatment of complex morphologies, such as the formation of voids during trench filling, but the motion of the interface is handled phenomenologically rather than physically, as by the phase field approach, so again the structure of the double layer is not considered. Bernard, Plapp, and Gouyet have recently presented a lattice-gas model of an electrochemical system [6,7] that exhibits many of the same interfacial and dynamic behaviors

*Electronic address: guyer@nist.gov
†Electronic address: william.boettinger@nist.gov
‡Electronic address: jwarren@nist.gov
§Electronic address: mcfadden@nist.gov

that we find in this paper, as well as exhibiting the early stages of dendritic growth. This type of discrete modeling should provide a useful bridge between an atomistic view of the electrochemical interface and the continuum approach of phase field models.

To place our results in context, Sec. II outlines the traditional sharp interface description of electrodeposition. Section III presents the dynamic postulates governing the evolution of the phase, concentration, and electrostatic potential fields which we proposed in Ref. [1]. Section IV describes our numerical approach and boundary conditions. Section V discusses the selection of materials parameters, including the relationship between the phase field mobility and the Butler-Volmer exchange current of traditional electrochemical modeling. Section VI presents the results of numerical calculations in one spatial dimension that span a range of electrodeposition and electrodissolution conditions.

II. SHARP INTERFACE APPROACH FOR ELECTRODEPOSITION

In Ref. [1], we present a phase field model of the equilibrium between an electrode phase α and an electrolyte phase β, consisting of a set of four charged components, e^-, M^{+m}, N^{+n}, and A^{-a}. A superscript α denotes that the quantity is evaluated in the bulk electrode (metal) phase and a superscript β denotes that the quantity is evaluated in the bulk electrolyte phase. At equilibrium, the difference in potential ϕ between the electrode and the electrolyte in an n-component system is given by

$$\Delta\phi = \phi^\alpha - \phi^\beta = -\frac{\Delta\mu_j^\circ}{z_i\mathcal{F}} + \frac{RT}{z_j\mathcal{F}}\ln\frac{X_j^\beta}{X_j^\alpha}, \quad j=1,...,n, \quad (1)$$

where $\Delta\mu_j^\circ = \mu_j^{\circ\alpha} - \mu_j^{\circ\beta}$ and μ_j° is the chemical potential of pure component j in the respective phase, z_j is the valence of component j, X_j is the mole fraction of component j, $\mathcal{F}$ is Faraday's constant, R is the molar gas constant, and T is temperature. Equation (1) is the generalization, for all of the components, of the Nernst equation of traditional electrochemical analysis. The equation is normally only written for the electroactive species. In Ref. [1] we explain the origin of an equation for each component in the system and the relationship between the term proportional to $\Delta\mu_j^\circ$ and the standard cell potential.

When current is passed through the interface, the potential difference $\Delta\phi$ shifts. Alternatively, when a potential difference other than the equilibrium value is imposed, current will pass and the interface will move. The shift in the potential difference across the interface (excluding the Ohmic drops across the bulk phases) is referred to as the overpotential η [8,9].

For an electrochemical system with only one monovalent electroactive species M^+, chemical reaction rate theory gives the relationship between current density i and total overpotential η for a planar interface as [8]

$$i = i_0\left\{\exp\left[\frac{(1-\nu)\mathcal{F}\eta}{RT}\right] - \frac{C_{M^+}}{C_{M^+}^\delta}\exp\left[-\frac{\nu\mathcal{F}\eta}{RT}\right]\right\}. \quad (2)$$

The first term in the curly brackets represents the anodic/oxidizing reaction and the second term represents the cathodic/reducing reaction. C_{M^+} is the concentration of cations M^+ in the electrolyte at electrode-electrolyte interface and $C_{M^+}^\delta$ is the bulk electrolyte concentration of cations M^+ at the edge of the diffusion boundary layer. The exchange current density i_0 and the transfer coefficient ν characterize the facility and symmetry of the forward and reverse reactions. The current density $i \equiv \mathbf{i}\cdot\mathbf{n}$, where the normal $\mathbf{n}$ points from α into β and $\mathbf{i}$ is the current density vector. Thus, positive values of i result in dissolution.

If the diffusion field can be assumed to be linear, the implicit dependence of C_{M^+} on i can be eliminated in Eq. (2), giving

$$i = i_0\left\{\exp\left[\frac{(1-\nu)\mathcal{F}\eta}{RT}\right] - \left(1-\frac{i}{i_{\lim}}\right)\exp\left[-\frac{\nu\mathcal{F}\eta}{RT}\right]\right\}. \quad (3)$$

This expression can be rearranged to give i as an explicit function of η, which is useful for comparison to our phase field results. Linearity of the concentration profile is appropriate only if the interface velocity is much less than D_{M^+}/δ_D, where D_{M^+} is the diffusivity of M^+ and δ_D is the thickness of the diffusion boundary layer. The limiting deposition current $i_{\lim}$ is determined by the complete depletion of M^+ in the electrolyte at the interface, such that

$$i_{\lim} = \frac{\mathcal{F}D_{M^+}C_{M^+}^\delta}{\delta_D} \quad (4)$$

The classical ''Butler-Volmer'' equation of electrochemistry is a special case of Eq. (3) in which the effects of mass transfer are neglected $(i/i_{\lim}\to 0)$.

For small overpotentials, the linearized form of Eq. (3) is

$$\eta \approx i\frac{RT}{\mathcal{F}}\left(\frac{1}{i_0} - \frac{1}{i_{\lim}}\right). \quad (5)$$

We will use this relationship in Sec. V C to relate i_0 to the parameters of our phase field model. When $|\eta|\mathcal{F}/RT \gg 1$ and $i \ll i_{\lim}$, Eq. (4) reduces to

$$i \approx i_0\exp\left[\frac{(1-\nu)\mathcal{F}\eta}{RT}\right] \quad \text{for} \quad \eta > 0 \quad (6a)$$

and

$$i \approx -i_0\exp\left[-\frac{\nu\mathcal{F}\eta}{RT}\right] \quad \text{for} \quad \eta < 0. \quad (6b)$$

The quantities $(1-\nu)\mathcal{F}/RT$ and $-\nu\mathcal{F}/RT$ are known as the anodic and cathodic ''Tafel slopes'' from the slopes of the lines when $\ln|i|$ is plotted against η. These slopes can be used to deduce experimental values for ν.

Equation (2) was originally derived from reaction rate theory to explain experimentally observed current-overpotential behavior. More recently, atomistic and quantum mechanical treatments of electron and ion transfer reactions have been performed to replace this chemical reaction

rate approach [10]. These treatments have led to a better physical understanding of the phenomenological constants ν and i_0, but they do not fundamentally alter the form of Eqs. (2) and (3).

III. MODEL

A. General kinetic equations

In Ref. [1], we performed a variational analysis to derive the governing equations for the equilibrium electrochemical interface. We also postulated the simplest time dependent forms of those governing equations that guarantee a decrease in total free energy with time *t*. We restate those dynamic postulates here. The time variation of the phase field ξ is given by

$$\frac{\partial \xi}{\partial t} = -M_\xi \left[\frac{\partial f_V}{\partial \xi} - \kappa_\xi \nabla^2 \xi - \frac{\epsilon'(\xi)}{2} (\nabla \phi)^2 \right], \tag{7}$$

where f_V is the Helmholtz free energy density per unit volume, κ_ξ is the phase field gradient energy coefficient, $\epsilon(\xi)$ is the dielectric constant, which we take to depend explicitly on the phase; because all of the fields are coupled, it will also depend implicitly on the electrolyte concentration. M_ξ is the mobility of the phase field. Under the assumption that all nonzero partial molar volumes are identical, the flux $\mathbf{J}_j$ of each component j is

$$\mathbf{J}_j = -M_j \nabla \left[\overline{\mu}_j - \frac{\overline{V}_j}{\overline{V}_s} \overline{\mu}_n \right], \quad j = 1,...,n-1, \tag{8}$$

where $\overline{\mu}_j$ is the electrochemical potential of species j and $\overline{V}_j$ is the partial molar volume of species j. We divide the components into electrons e^- with $j=1$, which have $\overline{V}_{e^-}=0$, and substitutional species with $j>1$, which all have the same $\overline{V}_j = \overline{V}_s = 0$. One consequence of this assumption is that $\Sigma_{j=2}^n C_j = \overline{V}_s^{-1} = \text{const}$, where C_j is the concentration of species j. A specific choice is made of a substitutional component n with nonzero partial molar volume to be called the reference species. The quantity M_j is the mobility of component j. Since conservation of species requires

$$\frac{\partial C_j}{\partial t} = -\nabla \cdot \mathbf{J}_j, \quad j = 1,...,n-1, \tag{9}$$

one obtains

$$\frac{\partial C_j}{\partial t} = \nabla \cdot \left\{ M_j \nabla \left[\overline{\mu}_j - \frac{\overline{V}_j}{\overline{V}_s} \overline{\mu}_n \right] \right\}, \quad j = 1,...,n-1. \tag{10}$$

Poisson's equation

$$\nabla \cdot [\epsilon(\xi) \nabla \phi] + \rho = 0 \tag{11}$$

must also be satisfied everywhere, where the charge density is

$$\rho = \mathcal{F} \sum_{j=1}^{n} z_j C_j. \tag{12}$$

The mobilities M_j and M_ξ will be related to the parameters of electrokinetics in Sec. V B and V C.

B. Form of the dynamic equations for ideal solution behavior

For simplicity, we assumed in Ref. [1] that the chemical part of the Helmholtz free energy per unit volume is described by an interpolation between two ideal solutions of the components,

$$f_V(\xi, C_j) = \sum_{j=1}^{n} C_j \{ \mu_j^{\circ\beta} + \Delta \mu_j^\circ p(\xi) + RT \ln C_j V_m + W_j g(\xi) \}, \tag{13}$$

where the molar volume $V_m = (\Sigma_{j=1}^n C_j)^{-1}$. We use an interpolating function $p(\xi) = \xi^3(6\xi^2 - 15\xi + 10)$ to bridge between the descriptions of the two bulk phases and a double-well function $g(\xi) = \xi^2(1-\xi)^2$ with a barrier height W_j for each component j to establish the metal/electrolyte interface [11]. The polynomials are chosen to have the properties that $p(0)=0$, $p(1)=1$, $p'(0)=p'(1)=0$, and $g'(0)=g'(1)=0$. The classical chemical potential is given by $\mu_j = \partial f_V / \partial C_j$ and the corresponding classical electrochemical potential is $\overline{\mu}_j = \mu_j + z_j \mathcal{F} \phi$.

Substituting Eq. (13) into Eqs. (7) and (8), we obtain the governing equation for evolution of the phase field under ideal solution thermodynamics

$$\frac{\partial \xi}{\partial t} = -M_\xi \left[p'(\xi) \sum_{j=1}^{n} C_j \Delta \mu_j^\circ + g'(\xi) \sum_{j=1}^{n} C_j W_j - k_\xi \nabla^2 \xi - \frac{\epsilon'(\xi)}{2} (\nabla \phi)^2 \right] \tag{14}$$

and the flux in the diffusion equation, Eq. (9), is given by

$$\mathbf{J}_j = -M_j \nabla \left[(\Delta \mu_j^\circ - \Delta \mu_n^\circ) p(\xi) + RT \ln \frac{C_j}{C_n} + (z_j - z_n) \mathcal{F} \phi + (W_j - W_n) g(\xi) \right], \quad j = 2,...,n-1, \tag{15a}$$

$$\mathbf{J}_{e^-} = -M_{e^-} \nabla \left[\Delta \mu_{e^-}^\circ p(\xi) + RT \ln \frac{\overline{V}_s C_{e^-}}{1 + \overline{V}_s C_{e^-}} + z_{e^-} \mathcal{F} \phi + W_{e^-} g(\xi) \right]. \tag{15b}$$

The flux of substitutional species does not explicitly depend on the electron concentration and the flux of electrons does not explicitly depend on the concentration of substitional species; the flux of substitutional species is affected by the displacement of other substitutional species, but electrons

can move without displacing other ions. The fluxes of all species are coupled indirectly through the total charge distribution and Eq. (11).

IV. NUMERICAL METHODS

The one-dimensional (1D) form of the governing equations was transformed to a frame moving at a velocity $\mathbf{v}$. Simulations were performed in a domain of length L with an initially abrupt interface between the bulk electrode and electrolyte phases at $x=L/2$, such that $\xi|_{x<L/2}=\xi^{\alpha}=1$ and $\xi|_{x>L/2}=\xi^{\beta}=0$. After choosing an initial bulk value for $C^{\beta}_{M^+}$, the remaining initial bulk C^{α}_j and C^{β}_j were the equilibrium values obtained by equating the bulk electrochemical potentials $\overline{\mu}_j$ [1]. The boundary condition on the phase field is $\mathbf{n}\cdot\nabla\xi=0$ at both ends of the solution domain. At the electrolyte end, we set $\phi=0$ and at the electrode end we specify i. At the leading edge of the moving frame, we model the stirred bulk electrolyte by applying a fixed concentration boundary condition. At the trailing edge of the frame, we discard the material leaving the frame by setting the divergence of the species fluxes to zero.

Equations (9), (11), (14), and (15) were solved with explicit finite differences. Spatial derivatives were taken to second order on a uniform mesh. Transient solutions were integrated numerically with an adaptive, fifth-order Runge-Kutta time stepper (based on ODEINT of Ref. [12]) until a steady state was achieved (current became constant). We have defined steady state in our simulations as the point when each $\mathbf{J}_j-\mathbf{v}C_j$ were uniform to within 0.1%. Because $\mathbf{v}$ is an unknown result of the simulation, the frame velocity was adjusted at each iteration to keep the interface stationary in the frame.

V. MATERIAL PARAMETERS

A. Equilibrium material parameters

We examine the dynamic behavior of a four component model under a different set of thermodynamic parameters than described in Ref. [1]. In this paper, all components have valence $z_j=\pm 1$. We are primarily interested in the electrodeposition of the more noble cation M^+, where the less noble cation N^+ and the anion A^- make up the bulk of the supporting electrolyte. This electrolyte containing only charged species represents a molten salt system. The presence of the second cation N^+ introduces the possibility of alloy deposition.

We take the partial molar volume of the "substitutional" components (M^+, N^+, and A^-) as $\overline{V}_s=10^{-5}$ m^3/mol. Equation (1) states that for any given X^{α}_j and X^{β}_j, there is some potential difference $\Delta\phi$ between that bulk phases that is related to the chemical potential difference of the pure components $\Delta\mu^{\circ}_j$. Conversely, we showed in Ref. [1] that we can establish a value for $\Delta\mu^{\circ}_j$ if we know $\Delta\phi$ for some particular X^{α}_j and X^{β}_j, for instance, the standard state values

$$\Delta\mu^{\circ}_j=RT\ln\frac{X^{\beta\circ}_j}{X^{\alpha\circ}_j}-z_j\mathcal{F}\Delta\phi^{\circ},\quad j=1,\ldots,n. \tag{16}$$

TABLE I. Numeric values of the potential-independent portion of the chemical potential differences $\Delta\mu^{\circ}_j$.

	$\ln(X^{\beta o}_j/X^{\alpha o}_j)$
e^-	−20.03
M^+	−3.912
N^+	20.01
A^-	20.03

The voltage-independent portion of $\Delta\mu^{\circ}_j$ is given in Table I. In this paper, we take $\Delta\phi^{\circ}$ to be zero. Following Ref. [1], this implies that the equilibrium state for this material system at the standard state concentration is near the point of zero charge. The mole fraction ratios in Table I of the normally electroinactive species are chosen to give the corresponding small standard state mole fractions as $X^{\beta\circ}_{e^-}=X^{\alpha\circ}_{N^+}=X^{\alpha\circ}_{A^-}=10^{-9}$.

To permit a convenient graphical display of bulk equilibrium, we invoke charge neutrality to transform the four components $\{e^-,M^+,N^+,A^-\}$ into an alternate set of four components that are charge neutral $\{M,N,MA,NA\}$. We plot the equilibrium phase diagram in terms of these transformed components in Fig. 1. Equilibrium states exist only between $-0.5138\ \text{V}<\Delta\phi<+0.1005$ V. It can be seen that over the majority of the potential range, from $-0.4\ \text{V}\lesssim\Delta\phi\lesssim 0$ V, the equilibrium is between an electrode of essentially pure M and a NA electrolyte containing a dilute concentration of MA. At the positive $\Delta\phi$ extreme, the equilibrium is between M

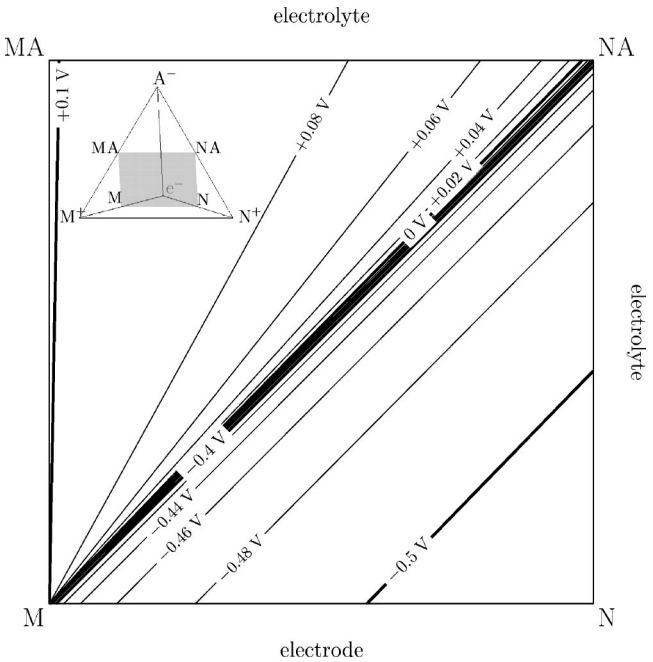

FIG. 1. Potential-composition phase diagram for the parameters in Table 1, illustrating the bulk equilibrium between a M electrode and an electrolyte containing MA salt dissolved in NA. Tie-lines denote different values of the quantity $(\Delta\phi-\Delta\phi^{\circ})$. The inset shows the position of this charge neutral phase diagram within the quaternary domain of the charged species.

TABLE II. Parameters characterizing the equilibrium interface. ϵ_0. is the permittivity of free space.

Parameter	Value
κ_ξ	7.2×10^{-11} J/m
$W_{j\in 2,\ldots,n}$	3.6×10^{5} J/mol
W_{e^-}	0 J/mol
ϵ	$8\epsilon_0$

and *MA* and at the negative $\Delta\phi$ extreme, the equilibrium is between a phase of *M* and *N* and a solution of *N* and *NA* for this choice of X_j°.

Table II lists our choice of the parameters that characterize the thickness and energy of the electrode-electrolyte interface. Our assumption that the barrier heights W_j are equal for the substitutional species and zero for electrons is discussed in Ref. [1].

B. Single phase transport properties (values for M_j)

To identify the mobilities M_j, we examine single-phase systems. In a single-phase electrode, $\xi=p(\xi)=1$. In a single-phase electrolyte, $\xi=p(\xi)=0$. In either phase $g(\xi)=\nabla p(\xi)=\nabla g(\xi)=0$. We thus can write the fluxes in Eq. (15) as

$$\mathbf{J}_j^{\text{bulk}}=-M_j\left[\frac{RT(C_n+C_j)}{C_nC_j}\nabla C_j+\frac{RT}{C_n}\sum_{\substack{i=2\\ i\neq j}}^{n-1}\nabla C_i+(z_j-z_n)\mathcal{F}\nabla\phi\right],\quad j=2,\ldots,n-1, \tag{17a}$$

$$\mathbf{J}_{e^-}^{\text{bulk}}=-M_{e^-}\left[\frac{RT\nabla C_{e^-}}{(1+\overline{V}_sC_{e^-})C_{e^-}}+z_{e^-}\mathcal{F}\nabla\phi\right]. \tag{17b}$$

The total current is given by the relationship

$$\mathbf{i}=\mathcal{F}\sum_{j=1}^{n}z_j\mathbf{J}_j. \tag{18}$$

The flux of component *n* balances the other fluxes such that

$$\sum_{j=2}^{n}\mathbf{J}_j=0. \tag{19}$$

We first consider an electrolyte with $\nabla\phi=0$. If we compare the resulting form of Eq. (17a) with the classical diffusive flux equation with diffusivities D_{ij},

$$\mathbf{J}_j=-\sum_{i=2}^{n-1}D_{ij}\nabla C_i,\quad j=2,\ldots,n-1 \tag{20}$$

the mobilities can be expressed in terms of the diagonal elements of D_{ij} as

$$M_j=\frac{D_{jj}C_nC_j}{RT(C_n+C_j)},\quad j=2,\ldots,n-1. \tag{21}$$

For simplicity, we assume the diagonal elements of D_{ij} are constants, thus inducing a concentration dependence in the mobilities as defined by Eq. (21) and in the off-diagonal D_{ij}'s.

We next consider an electrode with all $\nabla C_j=0$, where the current is entirely carried by the electromigration of electrons. The resulting form of Eq. (17b)

$$\mathbf{J}_{e^-}=-M_{e^-}z_{e^-}\mathcal{F}\nabla\phi \tag{22}$$

can be substituted into Eq. (18) to give

$$\mathbf{i}\approx-z_{e^-}^2\mathcal{F}^2M_{e^-}\nabla\phi. \tag{23}$$

By comparison with Ohm's law, $\mathbf{i}=-\sigma\nabla\phi$, we readily see that the electron mobility

$$M_{e^-}=\frac{\sigma}{z_{e^-}^2\mathcal{F}^2}=\frac{\sigma}{\mathcal{F}^2}. \tag{24}$$

Thus Eqs. (21) and (24) relate the M_j's to the electronic conductivity and ionic diffusivities.

On substitution of Eq. (21) into Eq. (17a), we see that the electromigration flux (due to gradients in ϕ) within the electrolyte is

$$\mathbf{J}_j^{\phi}=-M_j(z_j-z_n)\mathcal{F}\nabla\phi=-\frac{D_{jj}(z_j-z_n)C_nC_j\mathcal{F}}{RT(C_n+C_j)}\nabla\phi\approx-\frac{D_{jj}(z_j-z_n)C_j\mathcal{F}}{RT}\nabla\phi,\quad j=2,\ldots,n-1. \tag{25}$$

This is just as expected from traditional electrochemical theory, in the dilute limit where $C_n/(C_n+C_j)\approx1$. We will find in Sec. VIA that, for our supported ionic electrolyte and our electronic conducting electrode, the contributions of the electromigration current in the bulk electrolyte and of the diffusion current in the bulk electrode are indeed small.

It is interesting to note that the conductivity predicted by Eq. (24) is completely analogous to that predicted by the Drude model (and by the Fermi-Dirac model, for that matter) [13]

$$\sigma=\frac{z_{e^-}^2\mathcal{F}^2\tau C_{e^-}}{m_{e^-}}, \tag{26}$$

where m_{e^-} is the mass of the electron. The relaxation time τ can only be determined by quantum mechanical means and is simply an unknown constant in classical models of electron transport. Following an analysis for the electrons similar to that which gave us Eq. (21), we find that we can describe the mobility of electrons M_{e^-} in terms of a constant diffusivity of electrons D_{e^-},

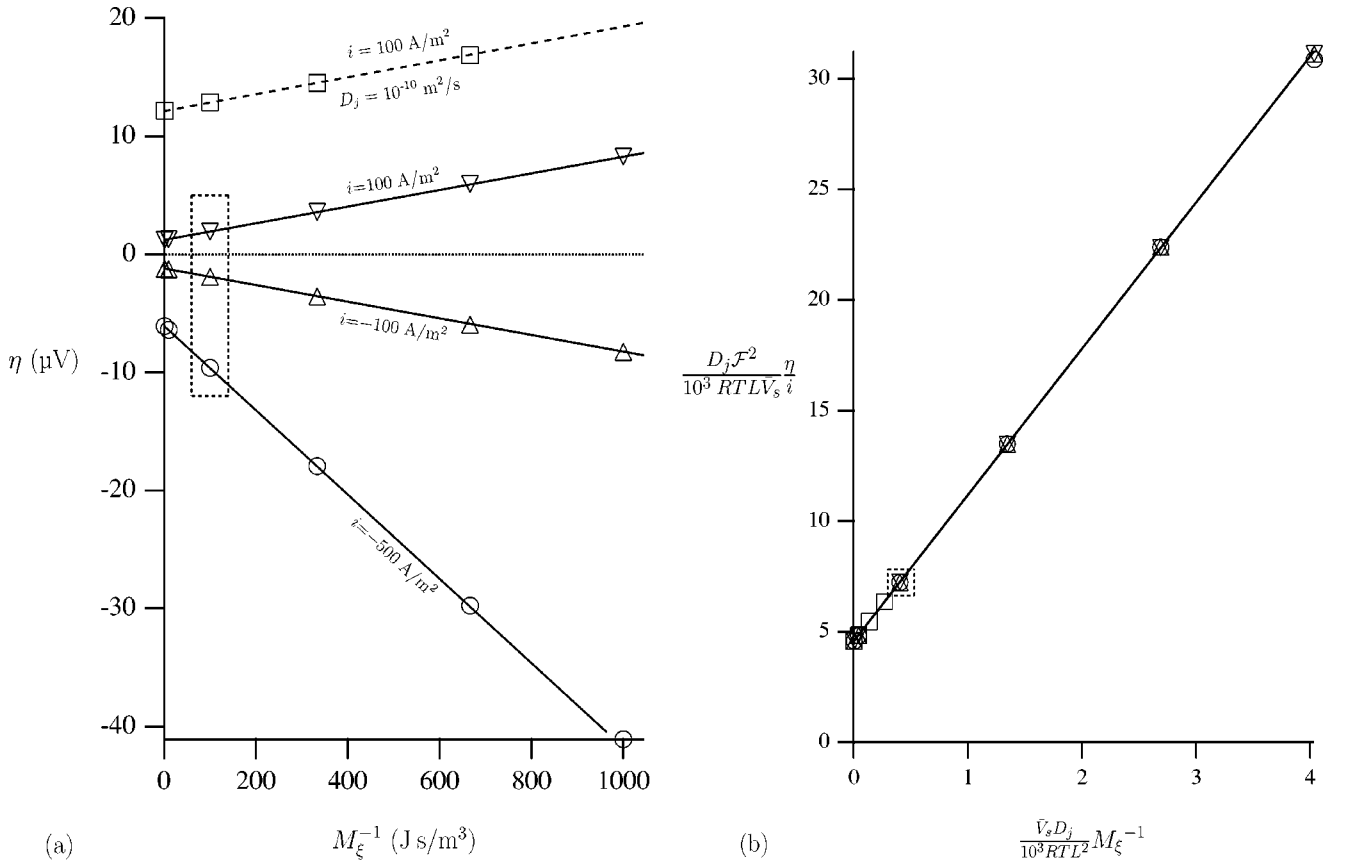

FIG. 2. (a) Dimensional and (b) dimensionless relationship between overpotential η and current i as a function of the inverse phase field mobility M_ξ^{-1} when $C^\beta_{M^+}=10$ mol/m^3 and $D_{jj}=10^{-9}$ m^2/s. Points are plotted for each permutation of $i=(-500,-100,100)$ A/m^2 and $M_\xi=(10^{-3},1.5\times10^{-3},3\times10^{-3},10^{-2},10^{-1},1)$ m^3/(J s). Points are also plotted for $i=100$ A/m^2 and $M_\xi=(1.5\times10^{-3},3\times10^{-3},10^{-2},1)$ m^3/(J s) with $D_{jj}=10^{-10}$ m^2/s. The line in (b) is a fit to $\eta/i=aM_\xi^{-1}+b$ with $a=(6.610\pm0.006)(\overline{V}_s^2/L\mathcal{F}^2)$ and $b=(4564\pm1)(RT\overline{V}_sL/D_{jj}\mathcal{F}^2)$. The points in the dotted box contribute to Fig. 5.

$$M_{e^-}=\frac{D_{e^-}(1+\overline{V}_sC_{e^-})C_{e^-}}{RT}. \tag{27}$$

In a single-phase conductor with uniform concentrations, $(1+\overline{V}_sC_{e^-})$ is a dimensionless constant of order 1. We can see that $D_{e^-}/(RT)$ is dimensionally equivalent to τ/m_{e^-} and all other terms in Eqs. (24) and (26) are identical. The room temperature conductivity of silver of approximately $6\times10^7\ \Omega^{-1}$ m^{-1} results in $D_{e^-}\approx8\times10^{-5}$ m^2/s and $M_{e^-}\approx6\times10^{-3}$ mol^2/(J s m). We observe that one of the weaknesses of the Drude model is that it fails to predict the $\sigma\sim T^{-1}$ dependence found in experiments without making some unsatisfactory *ad hoc* assumptions; this dependence arises naturally in our fundamentally thermodynamic formulation.

C. Interfacial kinetics (value for M_ξ)

Along with the transfer coefficient ν, the exchange current i_0 characterizes the kinetics of the interface and we hypothesize that it has an intimate relationship to the phase field mobility M_ξ. To test this hypothesis for our model, we examine Eq. (5) and plot η obtained from steady-state calculations against M_ξ^{-1} for various D_{jj} and small values of i in Fig. 2. If we scale length by L (the length of the solution domain), time by L^2/D_{jj}, energy density by $RT/\overline{V}_s$, and potential by $RT/\mathcal{F}$, we find that all of the points satisfy the linear relationship

$$\eta/i=(6.610\pm0.006)M_\xi^{-1}\frac{\overline{V}_s^2}{L\mathcal{F}^2}+(4563\pm1)\frac{RT\overline{V}_sL}{D_{jj}\mathcal{F}^2}. \tag{28}$$

Comparison with Eq. (5) reveals that

$$i_0=(0.1513\pm0.0001)M_\xi\frac{RT\mathcal{F}L}{\overline{V}_s^2}\approx3.62\times10^6\ \text{A/m}^2$$
$$\text{when}\ \ M_\xi=10^{-2}\ \text{m}^3/(\text{Js}) \tag{29}$$

and

$$i_{\lim}=(2.191\pm0.004)\times10^{-4}\frac{D_{jj}\mathcal{F}}{L\overline{V}_s}\approx2.11\times10^6\ \text{A/m}^2$$
$$\text{when}\ \ D_{jj}=10^{-9}\ \text{m}^2/\text{s}. \tag{30}$$

TABLE III. Correspondence between kinetic parameters used in this phase field model and those measured in experiments or typical of sharp-interface models. Typical physical values [9] are compared with the values used in our numerical calculations. The diffusivities are given for the electrolyte phase; diffusivities in the solid electrode are expected to be many orders of magnitude smaller. For the calculations in this paper, we treat the diagonal diffusivities as constant and uniform. To simplify the notation, we take $D_j \equiv D_{jj}$. No D_{A^-} is necessary because A^- is the reference species in our calculations.

Phase field	Physical	Numeric
$D_{e^-}=10^{-9}$ m^2/s	$\sigma=6\times10^{7}\ \Omega^{-1}$ m^{-1}	$\sigma=750\ \Omega^{-1}$ m^{-1}
$D_{M^+}=10^{-9}$ m^2/s	$D_{M^+}=10^{-9}$ m^2/s	$D_{M^+}=10^{-9}$ m^2/s
$D_{N^+}=10^{-9}$ m^2/s	$D_{N^+}=10^{-9}$ m^2/s	$D_{N^+}=10^{-9}$ m^2/s
$M_\xi=10^{-2}$ m^3/(J s)	$i_0=(10^{-16}$ to $10^{-2})$ A/cm^2	$i_0=3.7\times10^{6}$ A

Equation (29) confirms our hypothesis that i_0 is directly related to M_ξ. Comparing Eq. (30) to Eq. (4), and taking $C^\delta_{M^+}=10$ mol/m^3, we see that this implies that the diffusion boundary layer thickness is $\delta_D=(0.4564\pm0.0001)L$. This is very close to the thickness of the electrolyte, which validates that we are computing the diffusion field correctly (because we are modeling a diffuse interface, the electrolyte thickness is somewhat less than $0.5L$). The thinness of the diffusion boundary layer in our calculations gives rise to a limiting current that is much larger than encountered in physical systems, but the mechanism is the same.

Table III displays the kinetic parameters of the phase field model and typical values of the corresponding physical quantities. If physical values are used for some kinetic parameters, then the computation time is too long, so the values used for our numeric simulations are also listed.

VI. NUMERICAL RESULTS AND DISCUSSION

Our purpose is to show consistency of behavior with sharp interface models of electrochemical systems so that future 2D and 3D computations treating more complex phenomena can be performed with confidence. In this section, we examine the behavior of our model in the bulk phases, explore the current-overpotential behavior, and demonstrate the electrodeposition of alloys at high applied currents.

The interfacial region of a representative steady-state solution, with $i=-100$ A/m^2, is displayed in Fig. 3. The phase field ξ, concentrations C_j, charge density ρ, and electrostatic potential ϕ are plotted against the same x axis. The velocity of the moving frame is indicated with a marker on the ξ curve at $\xi=0.5$. To highlight the location of the interface, $g(\xi)$ is mapped onto the background in gray. We can see that the concentrations deviate from their bulk values in a region

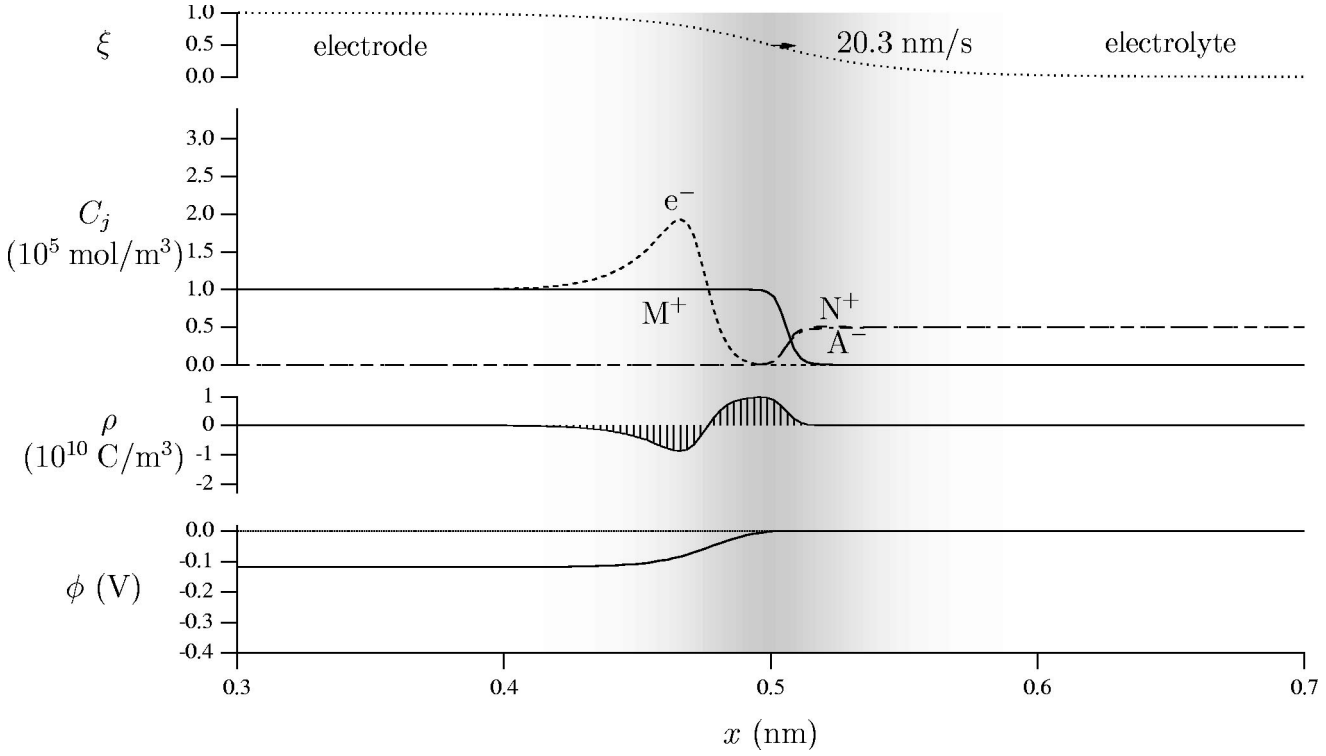

FIG. 3. Interface profiles for steady state electrodeposition with $i=-10^2$ A/m^2. The concentration profiles for N^+ and A^- are almost coincident on this scale. $g(\xi)$ is mapped onto the background in gray to indicate the location of the phase field interface.

TABLE IV. Partial fluxes in the bulk electrolyte for $i=-100$ A/m^2 (electrodeposition). $\nabla\phi=6.87\times10^{-4}$ V/m.

j	C_j (mol/m^3)	∇C_j (mol/m^4)	$\mathbf{J}_j^D$ (mol m^{-2} s^{-1})	$\mathbf{j}_j^\phi$ (mol m^{-2} s^{-1})	$\mathbf{j}_j^{\text{total}}$ (mol m^{-2} s^{-1})
e^-	1.00×10^{-2}	-1.65×10^{3}	1.65×10^{-6}	0	1.65×10^{-6}
M^+	1.00×10^{1}	1.03×10^{6}	-1.03×10^{-3}	0	-1.03×10^{-3}
N^+	5.00×10^{4}	-1.03×10^{6}	5.18×10^{-4}	-1.34×10^{-6}	5.16×10^{-4}
A^-	5.00×10^{4}	8.28×10^{2}			5.17×10^{-4}

of approximately the same thickness as the phase field transition. As a result, the charged ''double layer'' is confined to this same region. The surface of the electrode has excess e^-, whereas the surface of the electrolyte is an essentially charge-neutral *NA* salt with a dilute concentration of *MA*. All of the species except M^+ are excluded from the region of intermediate ξ, giving rise to a layer of M^+ that has neither e^- nor A^- to balance the charge. This charge distribution gives rise to the potential step of approximately 0.12 V between the two phases, which is the expected Nernst potential of an electrolyte with $C^\beta_{M^+}=10$ mol/m^3.

A. Fluxes

The relative contributions of the flux due to diffusion $\mathbf{J}_j^D$ (dependent on all the ∇C_i) and the flux due to electromigration $\mathbf{J}_j^\phi$ (proportional to $\nabla\phi$) can be distinguished using Eq. (17). For $i=-100$ A/m^2, the partial fluxes in the bulk electrolyte are listed in Table IV and those in the bulk electrode are listed in Table V. As the designated reference species, the flux of A^- always adjusts such that the sum of the fluxes of the substitutional species is zero. In both phases, the concentration gradients of M^+ and N^+ are approximately equal and opposite in sign to maintain charge neutrality (the concentration gradients of A^- and e^- are small). The diffusive fluxes of M^+ and N^+ are *not* equal and opposite in sign. The ''off-diagonal'' term for the N^+ flux in the electrode and for both the M^+ and N^+ fluxes in the electrolyte contribute significantly.

Because we consider a supported electrolyte (the total ion density is high), $\nabla\phi$ is small and electromigration does not contribute significantly to the current in the electrolyte. Both the magnitude and gradient of C_{e^-} are small in the electrolyte, such that e^- do not carry any significant current in the electrolyte. The current due to the N^+ flux is canceled by that due to the A^- flux, such that essentially all of the current in the electrolyte is carried by the diffusion of M^+. In the electrode, the partial fluxes of the substitutional components are numerically zero. The concentration gradient of e^- is small in the electrode, giving a small diffusive flux. The bulk of the current in the electrode is carried by electromigration of e^-, consistent with Ohm's law. These observations that the current in the electrolyte is carried by diffusion of M^+ and the current in the electrode is carried by the electromigration of e^- are consistent with the approximations we made for the bulk phases in Sec. V B; i.e., bulk behavior is obtained at a distance of 0.5 nm from the interface.

B. Diffusion layer

In Fig. 4 we plot the profile of M^+ in the electrolyte, showing the depletion due to electrodeposition and the enrichment due to electrodissolution. At the highest current in Fig. 4(a), we can see that C_{M^+} near the surface of the electrode is depleted practically to zero, giving rise to the limiting current behavior of Sec. II. The diffusion layer thickness $\delta_D=0.456L$, calculated in Sec. V C, is indicated for comparison. Over the range of applied currents examined, the enrichment of M^+ during electrodissolution is not similarly constrained.

C. Current-overpotential relationship

In Sec. V C, we found that the relationship between current i and overpotential η in our calculations is satisfied by the linear relationship (5) when i and η are small. Now we plot i versus η over a larger range of applied currents in Fig. 5 as open squares. Equation (3) considers only the electroactive species, so the filled circles in Fig. 5 show the current carried by the electroactive cation i_{M^+}. The relationship between i_{M^+} and η is not linear. At large, negative values of η, we observe a limiting current, whereas for large positive values of η, no such limiting current is observed and i_{M^+} appears exponentially dependent on η. We fit Eq. (3) to the calculated values of i_{M^+} and we find that $i_0=(3.80\pm0.08)\times10^6$ A/m^2, $i_{\text{lim}}=(-2.15\pm0.06)\times10^6$ A/m^2, and $\nu=0.777\pm0.002$. These values of i_0 and i_{lim} are within 5% of the values found in the linear analysis of Sec. V C. Because i_0 is of the same order as i_{lim} in our calculations, we do not ob-

TABLE V. Partial fluxes in the bulk electrode for $i=-100$ A/m^2 (electrodeposition). $\nabla\phi=0.133$ V/m.

j	C_j (mol/m^3)	∇C_j (mol/m^4)	$\mathbf{J}_j^D$ (mol m^{-2} s^{-1})	$\mathbf{j}_j^\phi$ (mol m^{-2} s^{-1})	$\mathbf{j}_j^{\text{total}}$ (mol m^{-2} s^{-1})
e^-	1.00×10^{5}	4.97×10^{2}	-4.97×10^{-7}	1.03×10^{-3}	1.03×10^{-3}
M^+	1.00×10^{5}	-5.93×10^{5}	1.85×10^{-7}	0	1.85×10^{-7}
N^+	2.04×10^{-2}	5.93×10^{5}	1.24×10^{-7}	0	1.24×10^{-7}
A^-	2.10×10^{-6}	1.88×10^{2}			-3.10×10^{-7}

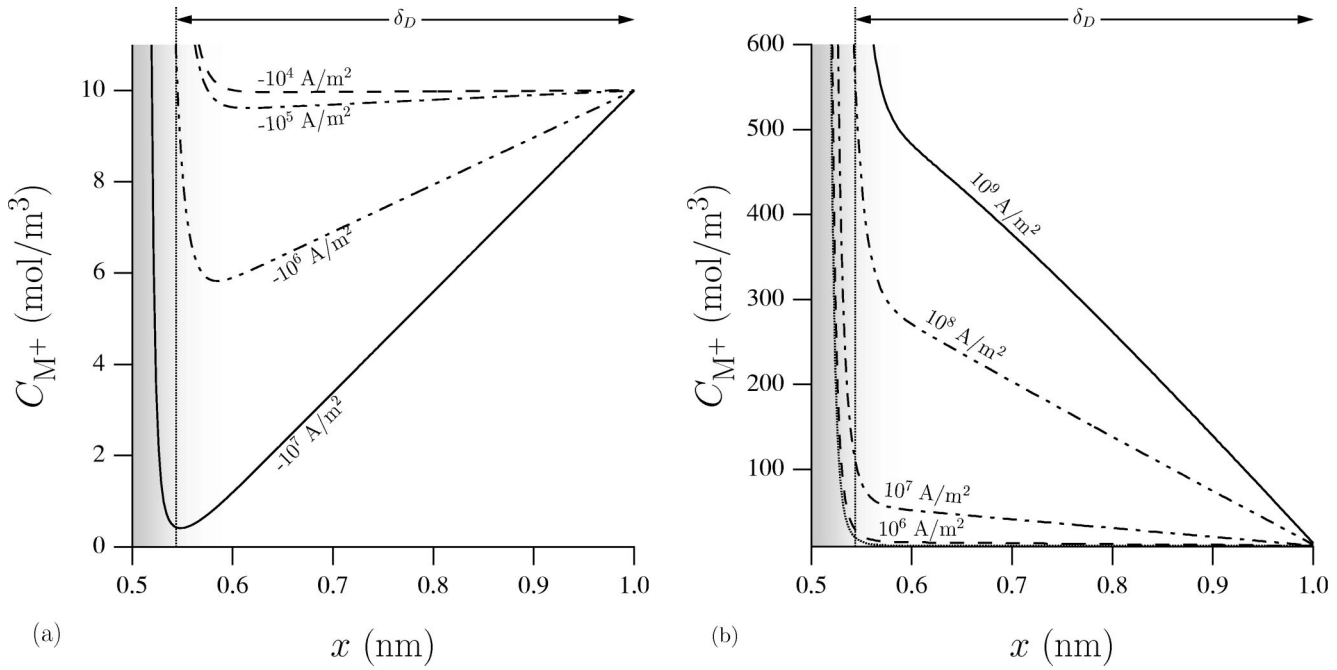

FIG. 4. Concentration of M^+ as a function of position in the electrolyte for different total (a) electrodeposition and (b) electrodissolution currents. The concentration at the interface exhibits a Nernstian shift in concentration with overpotential as the current is changed. The diffusion boundary layer is clearly linear over the small simulation domain. $g(\xi)$ is mapped onto the background in gray to indicate the location of the phase field interface. The dashed vertical line indicates the thickness of the diffusion boundary layer δ_D calculated in Sec. V C. The concentration gradient at $i=-10^7$ A/m^2 gives rise to the M^+ limiting current of $i_{\mathrm{lim}}\approx -2\times 10^6$ A/m^2; the majority of the current is carried by other species.

serve an obvious ''Tafel slope'' during electrodeposition. Nonetheless, the transition between low current and diffusion-limited current cannot be fit except by the full form of Eq. (3). From these results, we see that despite postulating a linear evolution equation for the phase field [Eq. (7)], we obtain the nonlinear current-overpotential behavior predicted by sharp-interface theories and observed in electrochemical experiments.

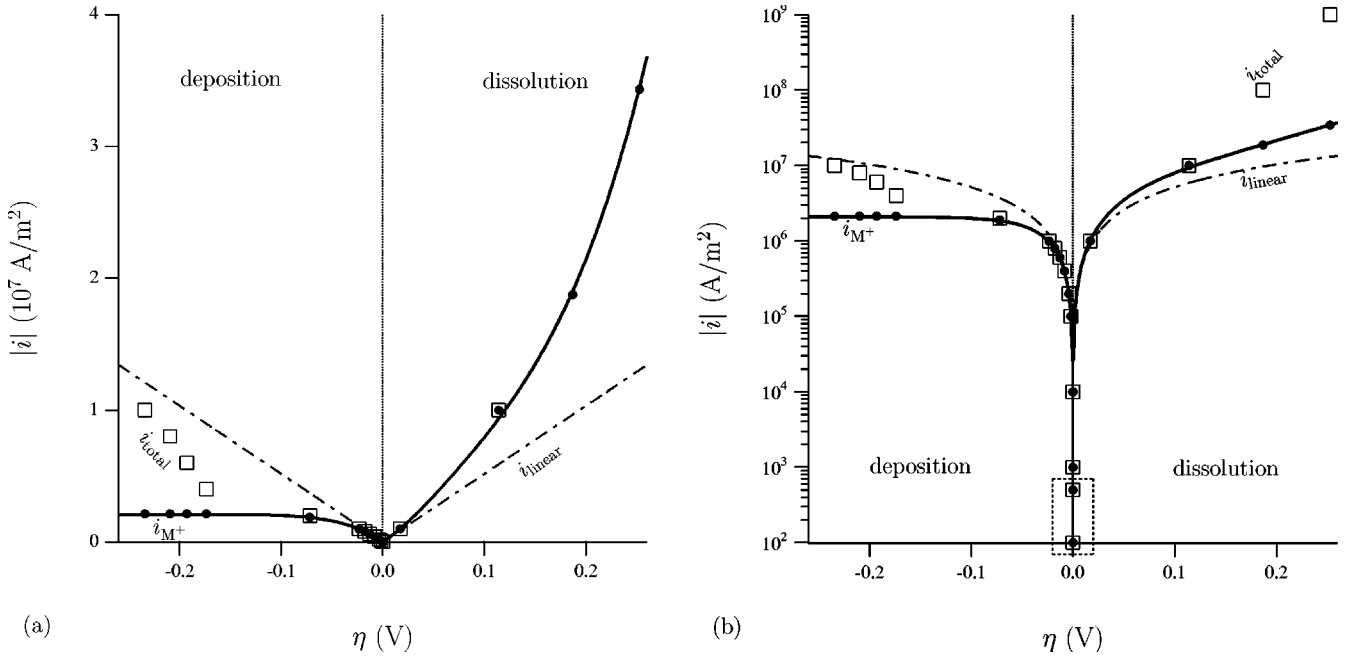

FIG. 5. Magnitude of the current i as a function of the overpotential η, plotted on (a) linear and (b) log-linear scales. The open squares indicate the total current and the circles indicate the partial current of M^+. The solid line is a plot of the current-overpotential equation (3) for $i_0=3.80\times 10^6$ A/m^2, $i_{\mathrm{lim}}=-2.15\times 10^6$ A/m^2, and $\nu=0.777$. The dashed line is a plot of the linear current-overpotential equation (5) for the same parameters. The dotted box indicates the points that contribute to Fig. 2.

The transfer coefficient ν characterizes the symmetry of the energy barrier between the electrode and electrolyte phases. A value of $\nu=0.5$ would mean the energy barrier is symmetric and that a given change in potential would cause the barrier to electrodeposition to change by the same magnitude as the barrier to electrodissolution. Our observed value of $\nu=0.78$ indicates that the barrier to electrodeposition is more sensitive to changes in potential than is the barrier to electrodissolution. Although we do not know the functional relationship between ν and the parameters of the phase field model, we can surmise that it is related to the height W_j and shape $g(\xi)$ of the interfacial energy barriers. This will be investigated in the future.

Since the exchange current is equal to the balanced anodic and cathodic current passed at equilibrium, it can be shown that [8,9]

$$i_0 \equiv k_0 \mathcal{F} C_0^{\infty(1-\nu)} C_R^{\infty\nu}. \tag{31}$$

C_O^∞ is the concentration of the oxidized electroactive species in the bulk electrolyte, which is $C_{M^+}^\beta = 10\ \mathrm{mol/m^3}$ in our notation. C_R^∞ is the concentration of the reduced electroactive species in the bulk electrode, which is $C_{M^+}^\alpha \approx 1/\overline{V}_s$ in our notation. The only terms we cannot directly identify in our phase field model are the dimensionless transfer coefficient ν and the rate constant k_0. Noting that we found $i_0 \propto M_\xi$ in Sec. V C, from a dimensional analysis, one may expect that

$$k_0 \propto M_\xi \gamma. \tag{32}$$

The surface free energy found in our paper on the equilibrium electrochemical interface [1] is

$$\gamma = \int_{-\infty}^{\infty} [\kappa_\xi (\xi')^2 - \epsilon (\phi')^2] dx. \tag{33}$$

From numerical calculations on the system in this paper when $i=0$, we obtain a value of $\gamma = 0.46\ \mathrm{J/m^2}$. If we assume that k_0 in Eq. (32) is not just proportional to but equal to $M_\xi \gamma$ and substitute this value of the surface free energy and Eq. (29) into Eq. (31), we obtain $\nu \approx 0.73$. If we assume instead that the surface free energy is that found in models of single component solidification [14]

$$\gamma = \sqrt{\frac{\kappa_\xi W}{18 \overline{V}_s}} = 0.38\ \ \mathrm{J/m^2}, \tag{34}$$

we find that $\nu \approx 0.75$. In either case, this value of ν is very close to that obtained by comparing our results to the sharp interface equation (3), and is not strongly sensitive to the choice of γ. Although ν is usually assumed to be 1/2 when no other information is available, it can take on any value between 0 and 1 for an ion transfer reaction [10].

D. Alloy electrodeposition

We examine electrodeposition of alloys by increasing the applied current by five orders of magnitude from $-10^2\ \mathrm{A/m^2}$ to $-10^7\ \mathrm{A/m^2}$, starting from the steady state result of Fig. 3. The fields in the vicinity of the interface are displayed at four different times in Fig. 6. We have added a small concentration inset to each frame to highlight the behavior of M^+ in the electrolyte and a bar of color that represents the overall composition of the system. The initial potential drop across the interface of $\Delta\phi = 0.118$ V is within 2 μV of the Nernst potential for $C_{M^+}^\beta = 10\ \mathrm{mol/m^3}$. At 10 ns after the step in current, C_{M^+} has depleted at the interface to approximately half its bulk value and N^+ has begun to accumulate at the electrode surface. At 200 ns, C_{M^+} has depleted essentially to zero at the electrode surface, giving rise to the limiting current of M^+ through the electrolyte. This M^+ current of approximately $-2.1\times10^6\ \mathrm{A/m^2}$ is not adequate to meet the applied current of $-10^7\ \mathrm{A/m^2}$. The surface of the electrode becomes covered with a layer very rich in N^+ and an alloy of M and N begins to deposit on the electrode. By 750 ns, the interfacial structure established at 200 ns is essentially unchanged and the original, pure M electrode has been completely swept from view, replaced by a MN alloy.

In Fig. 7, we plot the steady-state concentration of N^+ in the electrode as a function of η. For small overpotentials, up to $\eta \approx -0.17$ V, the electrode is essentially pure M. At large magnitudes of η, the fraction of N grows in an apparently linear fashion.

E. Interface structure

The concentration and charge distributions at the interface are sensitive to the electrodeposition conditions at all overpotentials or applied currents, but can be seen clearly in Fig. 6. At $i=-10^2\ \mathrm{A/m^2}$, C_{M^+}, C_{N^+}, and C_{A^-} in the electrolyte remain very close to their bulk values, all the way into the interfacial region. The charge distribution consists of a dipole on the electrode side, with very small net negative charge, and a corresponding positive charge on the electrolyte. At $i=-10^7\ \mathrm{A/m^2}$, C_{M^+} is depleted nearly to zero at the interface and N^+ displaces essentially all of the A^- at the interface. The density of e^- at the surface of the electrode is much larger than at the lower current and the charge distribution has shifted to a predominantly negative charge on the electrode and a positive charge on the electrolyte. These changes in the charge distribution are directly tied to the change in overpotential, through Eq. (11).

VII. CONCLUSIONS

Previously [1], we developed a phase field model of the electrochemical interface. We performed numerical calculations on a model system like an aqueous electrolyte, in which the majority species in the electrolyte had no charge. We demonstrated that, even with a simple ideal solution thermodynamic description, our model exhibited charged double layer behavior, an ''electrocapillary'' relationship between surface free energy and electrostatic potential difference across the interface, and differential capacitance curves that are strongly reminiscent of experimental measurements.

In this paper, we have applied the same phase field model to electrodeposition and electrodissolution conditions. We

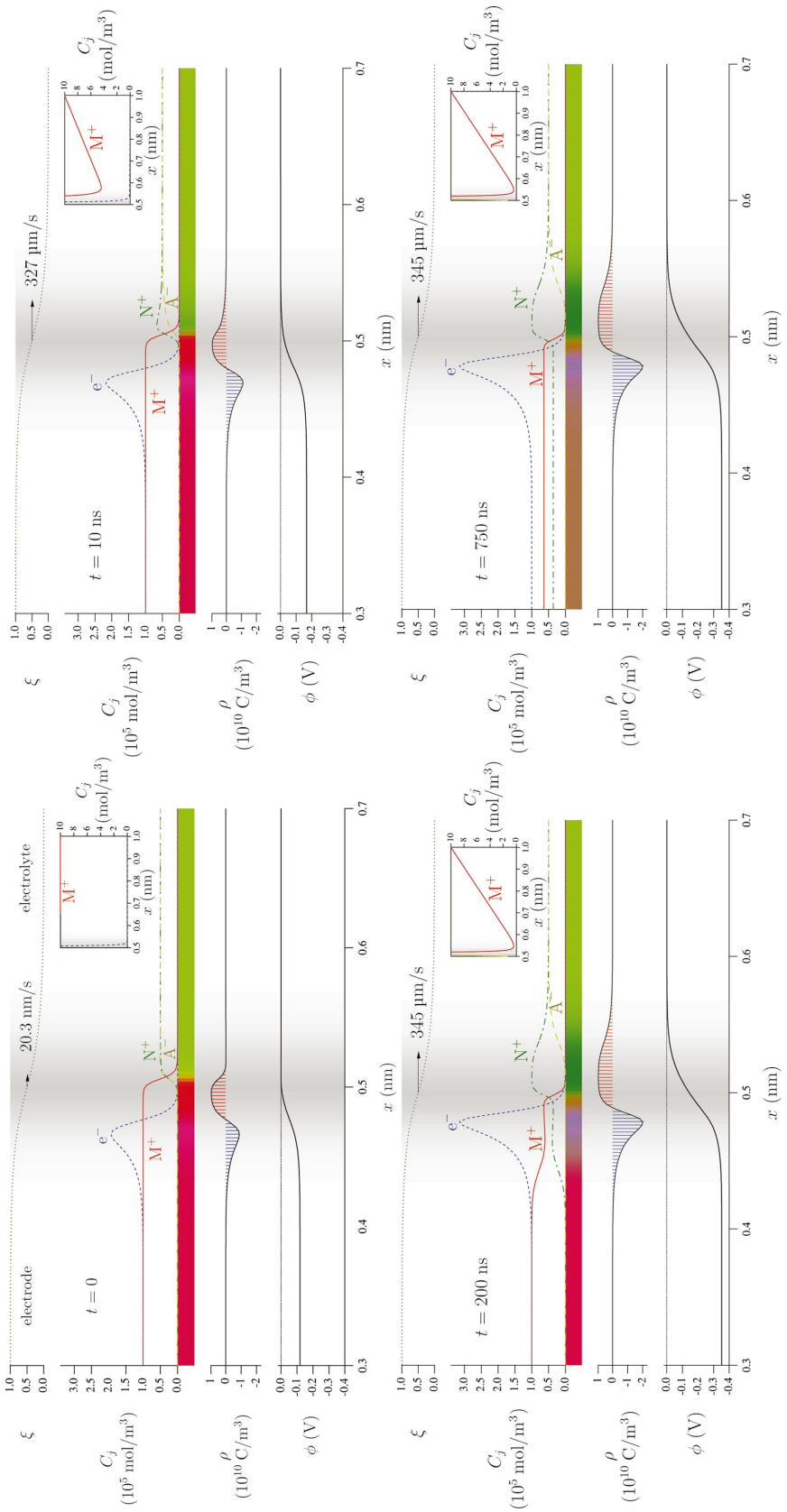

FIG. 6. (Color) Progress of alloy electrodeposition upon step from $i=-10^2$ A/m^2 to $i=-10^7$ A/m^2. $g(\xi)$ is mapped onto the background in gray to indicate the location of the phase field interface.

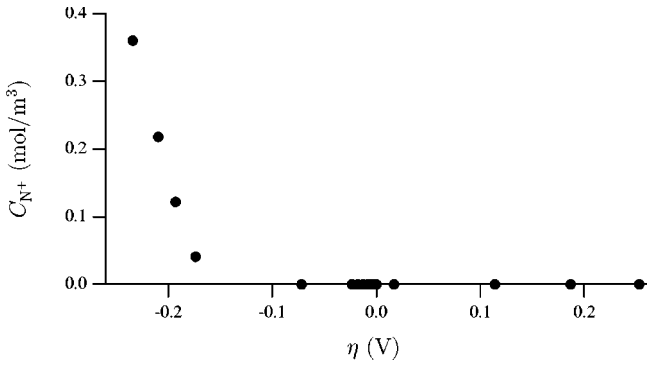

FIG. 7. Concentration C_{N^+} of N^+ in the deposited electrode as a function of overpotential η.

have performed numerical calculations on a model system like a molten salt, with four species which all carry charge. We have shown the following:

(1) The relationship between the parameters of the phase field model and the physical parameters of an electrochemical system.

(2) Our model electrode carries current by electromigration of electrons and that our model electrolyte carries current by diffusion of cations.

(3) The diffusion field in the electrolyte is essentially linear and that limiting current behavior results.

(4) Despite making linear postulates for the time-dependent governing equations, the current-overpotential relationship is nonlinear and agrees very well with the classic sharp-interface relationship (''Butler-Volmer'' with mass transport effects).

(5) Currents in excess of the limiting current for the more noble species result in the deposition of alloys.

(6) There are changes in the double layer structure with current.

As discussed in Ref. [1], the need to resolve the charge distribution in close proximity to the interface limits the size of the domain and the time spans we can model. Possibly, adaptive mesh techniques and implicit solution methods will enable us to examine larger domains and longer times. Nonetheless, our work here demonstrates that the phase field approach, using a very simple set of assumptions, can reproduce the rich behaviors of existing electrochemical theories and permit exploration of the relationship between double layer structure and interfacial kinetics.

ACKNOWLEDGMENTS

The authors are grateful for patient explanations of electrochemistry by U. Bertocci, E. Gileadi, T. P. Moffat, and G. R. Stafford; for helpful discussions regarding the modeling of phase transformations with J. W. Cahn, S. Coriell, A. Lobkovsky, R. F. Sekerka, and D. Wheeler; and for a careful reading of this manuscript by E. García. Part of this research was supported by the Microgravity Research Division of NASA.

[1] J. E. Guyer, W. J. Boettinger, J. A. Warren, and G. B. McFadden, Phys. Rev. E **69**, 021603 (2004).
[2] D. C. Grahame, Chem. Rev. (Washington, D.C.) **41**, 441 (1947).
[3] D. Dussault and A. Powell (unpublished).
[4] A. Powell and D. Dussault, in *Metallurgical and Materials Processing Principles and Technologies (Yazawa International Symposium)*, edited by H. Y. Sohn, K. Itagaki, C. Yamauchi, and F. Kongoli (TMS, Warrendale, PA, 2003), Vol. 3, pp. 235–250.
[5] D. Wheeler, D. Josell, and T. P. Moffat, J. Electrochem. Soc. **150**, C302 (2003).
[6] M.-O. Bernard, M. Plapp, and J.-F. Gouyet, in *Complexity and Fractals in Nature*, edited by M. M. Novak (World Scientific, Singapore, 2001), pp. 235–246.
[7] M.-O. Bernard, M. Plapp, and J.-F. Gouyet, Phys. Rev. E **68**, 011604 (2003).
[8] K. J. Vetter, *Electrochemical Kinetics: Theoretical and Experimental Aspects* (Academic, New York, 1967).
[9] A. J. Bard and L. R. Faulkner, *Electrochemical Methods: Fundamentals and Applications* (Wiley, New York, 2001).
[10] W. Schmickler, *Interfacial Electrochemistry* (Oxford University Press, New York, 1996).
[11] S.-L. Wang, R. Sekerka, A. A. Wheeler, B. T. Murray, S. R. Coriell, R. J. Braun, and G. B. McFadden, Physica D **69**, 189 (1993).
[12] W. H. Press, S. A. Teukolsky, W. T. Vetterling, and B. P. Flannery, *Numerical Recipes in C: The Art of Scientific Computing*, 2nd Ed. (Cambridge University Press, Cambridge, England, 1999).
[13] N. W. Ashcroft and N. D. Mermin, *Solid State Physics* (Saunders College, Philadelphia, PA, 1976).
[14] A. A. Wheeler, W. J. Boettinger, and G. B. McFadden, Phys. Rev. A **45**, 7424 (1992).